Lasers in Manufacturing Conference 2021

Laser in vacuum spot welding of electrical steel sheets with 3.7% Si-content

Krichel, T.[a,*], Olschok, S.[a], Reisgen, U.[a]

[a]*Welding and Joining Institute RWTH Aachen University, Pontstr. 49, 52062 Aachen, Germany*

Abstract

The energy efficiency of electric motors is largely determined by the magnetic and electrical properties of the soft magnetic core material. For high-frequency applications in the automotive sector, the cores usually consist of iron-silicon alloys with several lamellae electrically insulated from each other to minimize eddy current loss. To join these lamellae, a novel method with individual, statistically distributed weld spots instead of continuous linear welds is used. The influence of beam power and beam intensity on the weld geometry and grain structure of the material is investigated.

Keywords: laser in vacuum; electrical steel; spot welding

1. Introduction

The power density and energy efficiency of electrical machines is largely determined by the magnetic and electrical properties of the soft magnetic iron core material. Typically the cores are made up of several individual lamellae of iron-silicon alloys with a silicon content of up to 6.5 wt% [1–3]. For electrical insulation and corrosion protection, the lamellae are coated with an insulation coating in accordance with DIN EN 10342 [4; 5]. The shaping of the lamellae by punching or laser cutting inevitably leads to mechanically or thermally induced stresses and thus has negative effects on the magnetic properties of the material [6–10].

In iron cores made of electrical steel sheets, the combination of low electrical conductivity (high Si-content) and high inductance (lamellar structure) is used to reduce the losses during the remagnetization of the core and thus increase its efficiency [11; 12]. For joining the lamellae, adhesive bonding, stamping, punch-packing,

* *Corresponding author. Tel.: +49 241 80-96323*
E-mail address: krichel@isf.rwth-aachen.de

and welding have been established [13–15]. Each of these processes has a negative effect on the magnetic properties compared to a non-connected lamellae package [14], with bonding and stapling having the least influence [9]. However, the disadvantages of a low building factor and the cost intensive adhesive outweigh the advantages of bonding [15]. In the stamping process, the lamellae are deformed and stapled into each other. As a result the insulation layer is locally broken, which leads to short circuits and thus increased losses [14; 16]. The same applies to welding, which has so far only been used in the form of line welds to join the lamination stacks axially. In previous work it was found, that deterioration of the magnetic properties for line welding is higher than for spot welding [17]. Therefore a statistically equally distributed spot arrangement is investigated in this paper.

The heat input during welding also leads to changes in the grain structure and to residual stresses, both of which have a negative effect on the magnetic properties [14; 18–20]. In a current research project of the welding and joining institute (ISF) of RWTH Aachen University the aforementioned issues of welding are to be solved by the use of spot welds, which connect only 2-4 lamellae at a time. Laser beam welding in Vacuum (LaVa) is used for this purpose [21]. By means of individual small joints, short-circuit paths and welding residual stresses are to be induced only very locally, thus increasing the efficiency compared to line welds. This paper discusses the influence of beam power and beam intensity on the weld geometry and grain structure of the investigated material.

2. Materials and Methods

For the investigations in this paper two different laser systems were used (Fig. 1, left). A multi-mode disc laser (TRUMPF "TruDisc 16002") with a wavelength of 1030 nm and a single-mode fiber laser (IPG “YLS-2000-SM-Y16”) with a wavelength of 1070 nm. Both systems use optical fibers for beam guidance with a fiber diameter of 200 µm for the multi-mode and 35 µm for the single-mode laser. Both systems were used with an IPG „D50“ laser optic with a focusing length of 300 mm and an imaging ratio of 2:1. This results in a focus diameter of 400 µm for the multi-mode and 70 µm for the single-mode laser. The laser beam is guided by the laser optics into a vacuum chamber, which can generate a working pressure of 1 to 1000 mbar. A protective gas flow of argon is fed into the vacuum chamber to displace remaining atmosphere gases (Fig. 1, right).

type	energy distribution	wavelength [nm]	focus diameter [µm]	beam power [W]
multi-mode	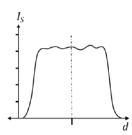	1030	400	320 – 16000
single-mode	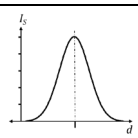	1070	70	200 – 2000

working pressure [mbar]	gas flow (Ar) [l/min]
1000	15
1	0.5

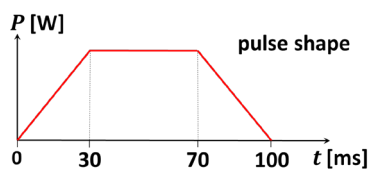

Fig. 1. Comparison of used laser beam systems (left); process parameters (right)

The used material M280-30AP [22; 23] is a soft magnetic iron-silicon alloy with 3.7 % Si-content. The average grain size $\bar{d}_K$ = 80 µm of the base material was determined using the line-cut method according to DIN EN ISO 634 [24].

The sheets have a thickness of 0.3 mm and are coated with an insulating varnish with a layer thickness of 2-10 µm. For the production of ring cores, the sheet was cut by laser beam cutting into annular lamellae with

an outer diameter d_E of 60 mm and an inner diameter d_I 48 mm (Fig. 2). A ring core consists of 30 lamellae, which are fixed and welded with a contact pressure of 0.1 N/mm². The defined contact pressure is sufficient to fix the lamellae without promoting pore formation [13]. Two joining strategies are investigated: line welds with continous wave beam and single spot welds with a pulse shape according to figure 1. In the case of line welds, 4 welds were made per core, each with 90° offset on the outer diameter, and all lamellae were joined axially.

In the case of spot welds, 4 welds were also made with 90° offset on the outer diameter, but this only connected 3-4 lamellae per spot. After this first plane has been welded, the ring is offset axially by 0.31 mm (a lamella width of 0.3 mm plus twice the average coating thickness) and turned radially by a defined angle afterwards 4 spot welds are applied again. Repeating this several times with different roation angles creates statistically equally distributed positions of the spot welds. The variing rotaion angles were calculated with the Latininized Centroidal Voronoi Tesselation Method (LCVT) [25].

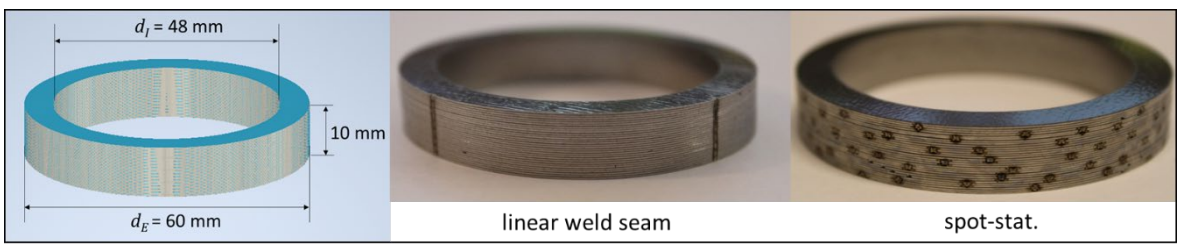

Fig. 2. From left to right: Schematic illustration of a ring core with 30 lamellas; linear weld seam; spot welds 10° offset; spot welds statistical distribution

During welding, the insulation coating evaporates due to the high energy input. There is a risk of seam defects such as pores and spatter as well as inclusions of non-evaporated insulation material. Carbon can be introduced into the melt and lead to hardening and a corresponding reduction in toughness [1; 12; 26].

3. Results and Discussion

Spot Welding. A quite high penetration depth occurred in cross sections 1 and 2 in Figure 3 due to the comparatively high power of 400 W in relation to the small focus diameter of only 70 µm with the single-mode laser. In addition, a finer grain structure occurred in cross-sections 1 and 2 compared to the base material. Large cross-sectional areas and changes in the grain structure compared to the base material can influence the mechanical and magnetic properties of the material and should therefore be avoided. This also applies to the coarse grain structure in cross section 4.

Finely dispersed impurities from the insulation coating promote fine grain formation (Fig. 3, detail of cross section 2), while the Si content reduced by burn-off can no longer suppress the precipitation of carbides, which accumulate at the grain boundaries and widen them. This increases the energy consumption for remagnetization and reduces the efficiency of the electric motor [12; 27–29].

With adjusted power, cross section 3 shows a homogeneous grain structure very similar to that of the base material and a filigree joining zone with a small joining cross section. The only disadvantage of this spot weld is the partial connection to the third lamella, which causes an unwanted short circuit. Even with optimized positioning, the slightly different layer thicknesses of the insulation can strongly influence the behavior of the melt and lead to undesired short circuits or seam defects such as spattering.

The grain structure in cross section 5 is also almost identical to that of the base material, but the cross-sectional area is significantly larger than in cross section 3 because of the bigger focus diameter of the multi-

mode laser (400 µm). In both parameter combinations, the insulation material evaporates in such a way that the melt is not contaminated or deformed. Deformation of the melt and a resulting reduced cross-sectional area occur at cross section 6. Here, the reduced power compared to cross section 5 is insufficient and the small melt volume solidifies before the evaporated insulation material can outgas.

The used multi-mode laser has a minimum power of 320 W. Therefore, a comparison of lower power ranges was not possible. The used single-mode laser can operate with only 200 W, which leads to a homogeneous grain structure and a small cross-sectional area in cross section 7 at reduced working pressure of 1 mbar. With the same power, cross section 8 shows a significant influence on the grain structure and the joining geometry as well as isolated pores at atmospheric pressure. It is assumed, that the evaporating insulation material cannot outgas fast enough and contaminates the melt.

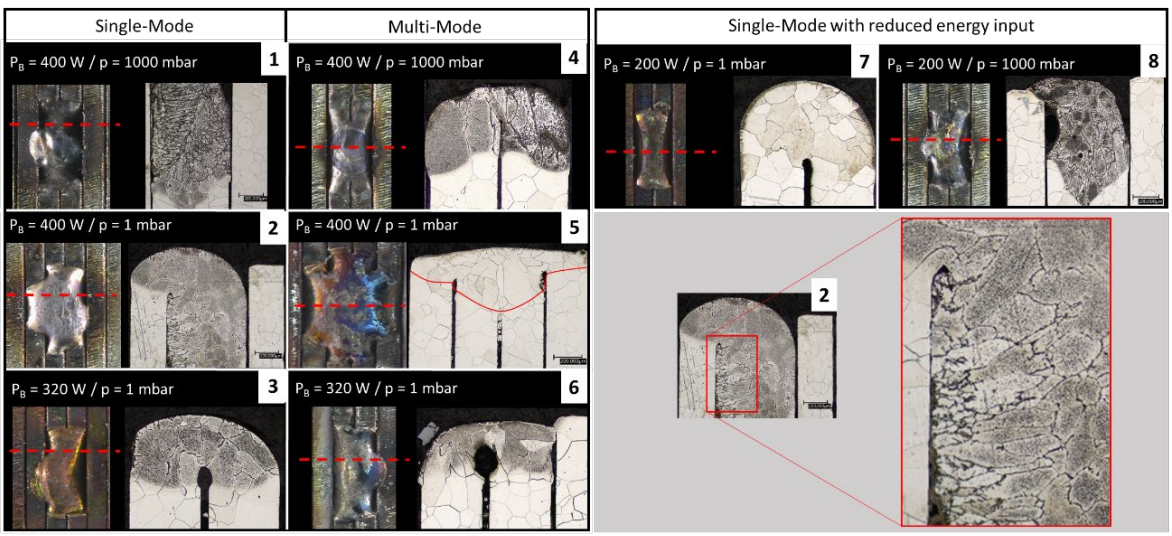

Fig. 3. Comparison of selected cross sections

Line Welding. The line welding was performed at a working pressure of 1 mbar for both laser types. The multi-mode laser created a weld width B of 0.66 mm with a beam power of 375 W at a welding speed of 2.2 m/min (Fig. 4). The grain structure is quite similar to the base material with an increase of $\bar{d}_K$ to about 110 µm. The small focus diameter of the single-mode laser results in a higher intensity in contrast to the multi-mode laser. Therefore the beam power and welding speed was reduced to 200 W and 0.1 m/min respectively. Additionally a circular beam oscillation with an amplitude of 0.5 mm and a frequency of 100 Hz was necessary to create a uniform weld seam with a width of 0.76 mm. On the one hand the single-mode reduced the penetration depth slightly to 0.39 mm in contrast to 0.45 mm with the multi-mode laser. On the other hand the cross section shows, that the insulation material between the lamellae contaminated the melt (Fig. 4, right).

It is assumed, that the carbon-based insulation coating induces carbon into the melt, which causes a very fine grain structure. Above the lamella appears a structure with dark coloured inclusions in a brighter coloured base material matrix. The hardness in this area is in the range of about 400 HV0.1 (Fig.5, left), which is already slightly above the hardness of the base material of about 240 HV0.1. Directly above the insulation coating between the lamellae appears an even finer grained structure with hardness up to 800 HV0.1. Regarding the slope-out area in Figure 5 (right), in which the beam power is decreased linear to zero to avoid an end crater,

the influence of the coating gets more obvious. With decreasing beam power the amount of dark hard-phases is reduced to zero above the last connected lamella where the melt shows no contamination of the coating. Lower beam power could not be investigated with the used beam sources. However, a lower beam power is not expected to create a significant benefit, because a coherent line weld inevitably melts parts of the insulation coating. The higher energy intensity with the smaller focal diameter of the single-mode laser is the most probable reason for this phenomenon, which did not appear with the multi-mode laser at any working pressures.

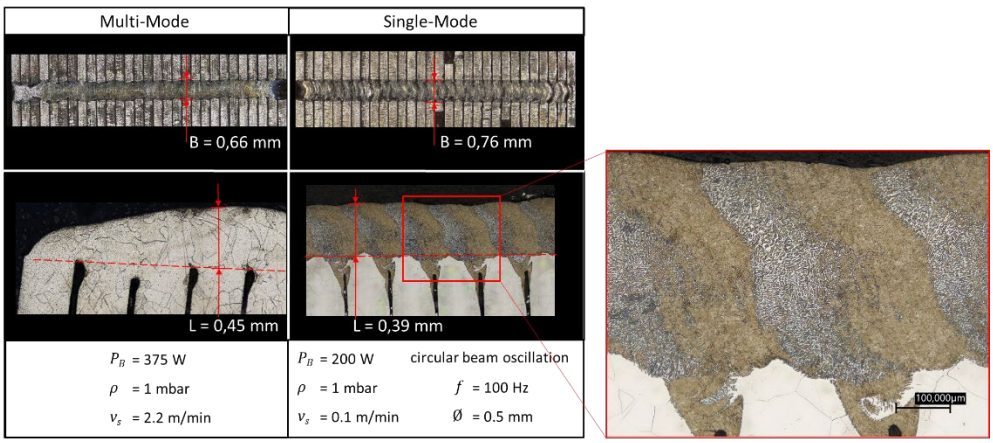

Fig. 4. Cross section for line welds of multi-mode (left) and single-mode (middle); detail of single-mode line weld (right)

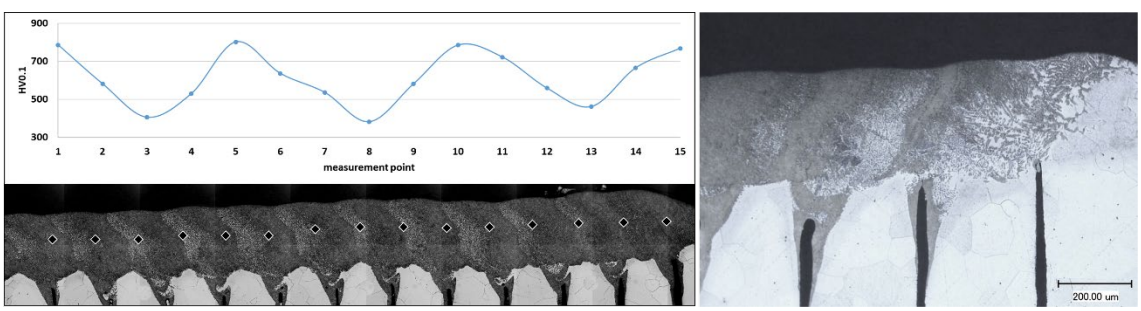

Fig. 5. Hardness HV0.1 of single-mode line weld (left); cross section of slope-out area (right)

4. Conclusion

The weldability of soft magnetic iron-silicon alloy M280-AP was investigated using a single-mode fibre laser with a focal diameter of 70 µm and a multi-mode disc laser with focal diameter of 400 µm with linear welds seams and single spot welds. A reduced working pressure was identified as major impact factor to the weldability. High quality line welds and spot welds were created at a working pressure of 1 mbar with both focal diameters.

The insulation coating between the lamellae is essential for the efficiency of electrical machines and can therefore not be removed. It was shown, that evaporating coating can cause deformations of the melt. But more important is the influence of the coating, which gets meddled into the melt and causes hard phases with a hardness of up to 800 HV0.1.

The influence of the working pressure is remarkable. Only at reduced working pressure of 1 mbar it was possible to create spot welds with minimized short circuits and minor changes in grain structure.

Acknowledgements

The presented investigations were carried out at RWTH Aachen University and funded by the Deutsche Forschungsgemeinschaft e.V. (DFG, German Research Foundation). The sponsorship and support is gratefully acknowledged.

References

[1] Ziegler, M. e. a. (2019): Potentials of Process Monitoring During Laser Welding of Electrical Steel Laminations. In: *9th International Electric Drives Production Conference (EDPC)*. DOI: 10.1109/EDPC48408.2019.9011918.

[2] Liang, Y. F. et al. (2010): Effect of annealing temperature on magnetic properties of cold rolled high silicon steel thin sheet. In: *Journal of Alloys and Compounds* (491), pp. 268–270. DOI: 10.1016/j.jallcom.2009.10.118.

[3] DIN EN 60404-1 (2017): Magnetische Werkstoffe - Teil 1: Einteilung. Beuth Verlag, Berlin.

[4] DIN EN 10342 (2005): Magnetische Werkstoffe - Einteilung der Isolationen auf Elektroblech. Beuth Verlag, Berlin.

[5] Brachthäuser, N. (2012): Elektromobilität–Neue Herausforderungen an den Werkstoff Elektroband. TU Darmstadt, 07.03.2012.

[6] Moses, A. J. et al. (2000): Aspects of the cut-edge effect stress on the power loss and flux density distribution in electrical steel sheets. In: *J. Magn. Magn. Mater.* (vol. 215/216), pp. 690–692. DOI: 10.1016/S0304-8853(00)00260-2.

[7] Maurel, V., F. Ossart, und R. Billardon (2003): Residual stresses in punched laminations: Phenomenological analysis and influence on the magnetic behavior of electrical steels. In: *J. Appl. Phys.* (vol. 93, no. 10), 7106–7108. DOI: 10.1063/1.1557279.

[8] Vandenbossche, L. e. a. (2013): Iron loss modelling which includes the impact of punching, applied to high efficiency induction machines. In: *Proc. 3rd Int. Elect. Drives Prod. Conf.*, pp. 1–10. DOI: 10.1109/EDPC.2013.6689720.

[9] Schoppa, A. P. et al. (2003): Influence of welding and sticking of laminations on the magnetic properties of non-oriented electrical steels. In: *J. Magn. Magn. Mater.*, 367-369. DOI: 10.1016/S0304-8853(02)00877-6.

[10] Imamori, S., S. Steentjes und K. Hameyer (2017): Influence of Interlocking on Magnetic Properties of Electrical Steel Laminations. In: *IEEE Trans. Magn.* 53 (11), pp. 1–4. DOI: 10.1109/TMAG.2017.2713446.

[11] Schneider, M., N. Urban und J. Franke (2017): Relation of joining parameters of stator core production and iron loss. DOI: 10.1109/EDPC.2017.8328148.

[12] Schade, T., R. M. Ramsayer und J. P. Bergmann (2014): Laser welding of electrical steel stacks - investigation of the weldability. In: *4th International Electric Drives Production Conference (EDPC)*, pp. 1–6. DOI: 10.1109/EDPC.2014.6984386.

[13] Schade, T. e. a. (2014): Electrical steel stacks for traction motors - fundamental investigation of the weldability. In: *Shaping the Future by Engineering: Proceedings; 58th IWK, Ilmenau Scientific Colloquium, Vol. 58*.

[14] Lamprecht, E., M. Hömme und T. Albrecht (2012): Investigations of eddy current losses in laminated cores due to the impact of various stacking processes. In: *2nd International Electric Drives Production Conference (EDPC)*, pp. 1–8. DOI: 10.1109/EDPC.2012.6425097.

[15] Wang, H., Y. Zhang und S. Li (2016): Laser welding of laminated electrical steels. In: *Journal of Materials Processing Technology* (vol. 230), pp. 99–108. DOI: 10.1016/j.jmatprotec.2015.11.018.

[16] Kurosaki, Y. e. a. (2008): Importance of punching and workability in non-oriented electrical steel sheets. In: *Journal of Magnetism and Magnetic Materials* 320 (20), pp. 2474–2480. DOI: 10.1016/j.jmmm.2008.04.073.

[17] Ukwungwu, D. e. a. (2020): Electromagnetic assessment of welding processes for packaging of electrical sheets. ISBN: 978-1-7281-8457-9. In: *10th International Electric Drives Production Conference (EDPC)*, pp. 156–161.

[18] Vourna, P. (2014): Characterization of Electron Beam Welded Non-Oriented Electrical Steel with Magnetic Barkhausen Noise. In: *Key Engineering Materials* (vol. 605), pp. 39–42. DOI: 10.4028/www.scientific.net/KEM.605.39.

[19] Schoppa, A. P., J. Schneider und C.-D. Wuppermann (2000): Influence of the manufacturing process on the magnetic properties of non-oriented electrical steels. In: *Journal of Magnetism and Magnetic Materials* 215-216, pp. 74–78. DOI: 10.1016/S0304-8853(00)00070-6.

[20] Radaj, D. (2002): Eigenspannungen und Verzug beim Schweißen: Rechen- und Messverfahren, DVS-Verlag, Fachbuchreiche Schweißtechnik (Bd. 143), ISBN 3-87155-194-5.

[21] Jakobs, S. (2015): Laserstrahlschweißen im Vakuum: Erweiterung der Prozessgrenzen für dickwandige Bleche [Dissertation]. RWTH Aachen. Aachen: Shaker Verlag. ISBN: 978-3-8440-4032-6.

[22] DIN EN 10027-1 (2017): Bezeichnungssysteme für Stähle - Teil 1: Kurznamen. Beuth Verlag, Berlin.

[23] DIN EN 10106 (2016): Kaltgewalztes nicht kornorientiertes Elektroband und -blech im schlussgeglühten Zustand. Beuth Verlag, Berlin.
[24] DIN EN ISO 643 (2020): Stahl – Mikrophotographische Bestimmung der erkennbaren Korngröße. Beuth Verlag, Berlin.
[25] Romero, V., J. Burkardt, G. M. und J. Peterson (2006): Comparison of pure and "Latinized" centroidal Voronoi tesselation against various other statistical sampling methods. In: *Journal of Reliability Engineering and system Safety*, pp. 1266–1280. DOI: 10.1016/j.ress.2005.11.023.
[26] Brachthäuser, N. e. a. (2011): Laserstrahlschweissen von paketierten Elektroblechen. In: *ATZproduktion 4.3*, pp. 38–43. DOI: 10.1365/s35726-011-0042-5.
[27] Traint, S. e. a. (2002): Influence of silicon, aluminium, phosphorus and copper on the phase transformations of low alloyed TRIP-steels. In: *Steel Research* 73 (6-7), pp. 259–266. DOI: 10.1002/srin.200200206.
[28] Petrovic, D. S. (2010): NON-ORIENTED ELECTRICAL STEEL SHEETS. In: *Materials and technology 44*, pp. 317–325.
[29] Delagnes, D. e. a. (2005): Influence of silicon content on the precipitation of secondary carbides and fatigue properties of a 5%Cr tempered martensitic steel. In: *Materials Science and Engineering: A* 394 (1-2), pp. 435–444. DOI: 10.1016/j.msea.2004.11.050.